Characterizing and tracking individual colloidal particles using Fourier-Bessel image decomposition

Filip Strubbe,[1,2,*] Stijn Vandewiele,[1,2] Caspar Schreuer,[1,2] Filip Beunis,[1,2] Oksana Drobchak,[1,2] Toon Brans,[1,2] and Kristiaan Neyts[1,2]

[1]*Electronics and Information Systems, Ghent University, Sint-Pietersnieuwstraat 41, Ghent B-9000, Belgium*
[2]*Center for Nano and Biophotonics (NB-Photonics), Ghent University, Sint-Pietersnieuwstraat 41, Ghent B-9000, Belgium*
[*]*filip.strubbe@elis.ugent.be*

Abstract: We use Fourier-Bessel Image Decomposition (FBID) of microscopy images to investigate the size, refractive index and 3-dimensional position of individual colloidal microspheres. With measurements of monodisperse polystyrene and poly(methyl methacrylate) particles we achieve a resolution of 1% in size and 0.2% in refractive index for a single image which is sufficient for accurate in situ characterization of polydisperse colloids. Also the binding of avidin molecules to individual biotinylated polystyrene particles is resolved. Finally, the FBID method offers a straightforward approach to 3-dimensional out-of-focus tracking. Here, the *z*-position of a freely diffusing particle is calculated by applying the statistics of Brownian motion to its set of Fourier-Bessel coefficients.

OCIS codes: (100.1830) Deconvolution; (110.2960) Image analysis.

References and links

1. F. Caruso, "Nanoengineering of particle surfaces," Adv. Mater. **13**(1), 11–22 (2001).
2. S. Derveaux, B. G. Stubbe, C. Roelant, M. Leblans, B. G. De Geest, J. Demeester, and S. C. De Smedt, "Layer-by-layer coated digitally encoded microcarriers for quantification of proteins in serum and plasma," Anal. Chem. **80**(1), 85–94 (2008).
3. D. A. A. Vignali, "Multiplexed particle-based flow cytometric assays," J. Immunol. Methods **243**(1–2), 243–255 (2000).
4. R. Galneder, V. Kahl, A. Arbuzova, M. Rebecchi, J. O. Rädler, and S. McLaughlin, "Microelectrophoresis of a bilayer-coated silica bead in an optical trap: application to enzymology," Biophys. J. **80**(5), 2298–2309 (2001).
5. H. Shpaisman, B. J. Krishnatreya, and D. Grier, "Holographic microrefractometer," Appl. Phys. Lett. **101**(9), 091102 (2012).
6. E. A. Abbondanzieri, W. J. Greenleaf, J. W. Shaevitz, R. Landick, and S. M. Block, "Direct observation of base-pair stepping by RNA polymerase," Nature **438**(7067), 460–465 (2005).
7. S. Stotz, "Field dependence of the electrophoretic mobility of particles suspended in low-conductivity liquids," J. Colloid Interface Sci. **65**(1), 118–130 (1978).
8. A. R. M. Verschueren, L. W. G. Stofmeel, P. J. Baesjou, M. H. W. M. van Delden, J. J. van Glabbeek, K.-M. H. Lenssen, M. Mueller, J. T. M. Osenga, G. Oversluizen, and R. M. Schuurbiers, "Optical performance of in-plane electrophoretic color E-paper," J. SID **18**, 1 (2007).
9. M. Humar, M. Ravnik, S. Pajk, and I. Muševič, "Electrically tunable liquid crystal optical microresonators," Nat. Photon. **3**(10), 595–600 (2009).
10. N. M. Hanumegowda, C. J. Stica, B. C. Patel, I. White, and X. Fan, "Refractometric sensors based on microsphere resonators," Appl. Phys. Lett. **87**(20), 201107 (2005).
11. A. Yethiraj and A. van Blaaderen, "A colloidal model system with an interaction tunable from hard sphere to soft and dipolar," Nature **421**(6922), 513–517 (2003).
12. M. Medebach and T. Palberg, "Phenomenology of colloidal crystal electrophoresis," J. Chem. Phys. **119**(6), 3360–3370 (2003).
13. K. Braeckmans, K. Buyens, W. Bouquet, C. Vervaet, P. Joye, F. De Vos, L. Plawinski, L. Doeuvre, E. Angles-Cano, N. N. Sanders, J. Demeester, and S. C. De Smedt, "Sizing nanomatter in biological fluids by fluorescence single particle tracking," Nano Lett. **10**(11), 4435–4442 (2010).
14. J. A. Gallego-Urrea, J. Tuoriniemi, and M. Hassellöv, "Applications of particle-tracking analysis to the determination of size distributions and concentrations of nanoparticles in environmental, biological and food samples," Trends Analyt. Chem. **30**(3), 473–483 (2011).

#220421 - $15.00 USD Received 5 Aug 2014; revised 17 Sep 2014; accepted 21 Sep 2014; published 1 Oct 2014

15. N. Garbow, J. Müller, K. Schätzel, and T. Palberg, "High-resolution particle sizing by optical tracking of single colloidal particles," Physica A **235**(1–2), 291–305 (1997).
16. S. H. Lee, Y. Roichman, G. R. Yi, S. H. Kim, S. M. Yang, A. van Blaaderen, P. van Oostrum, and D. G. Grier, "Characterizing and tracking single colloidal particles with video holographic microscopy," Opt. Express **15**(26), 18275–18282 (2007).
17. E. Darakis, T. Khanam, A. Rajendran, V. Kariwala, T. J. Naughton, and A. K. Asundi, "Microparticle characterization using digital holography," Chem. Eng. Sci. **65**(2), 1037–1044 (2010).
18. J. C. Crocker and D. G. Grier, "Methods of digital video microscopy for colloidal studies," J. Colloid Interface Sci. **179**(1), 298–310 (1996).
19. Y. Feng, J. Goree, and B. Liu, "Accurate particle position measurement from images," Rev. Sci. Instrum. **78**(5), 053704 (2007).
20. M. C. Jenkins and S. U. Egelhaaf, "Confocal microscopy of colloidal particles: Towards reliable, optimum coordinates," Adv. Colloid Interface Sci. **136**(1–2), 65–92 (2008).
21. F. C. Cheong, B. Sun, R. Dreyfus, J. Amato-Grill, K. Xiao, L. Dixon, and D. G. Grier, "Flow visualization and flow cytometry with holographic video microscopy," Opt. Express **17**(15), 13071–13079 (2009).
22. Y. Park, G. Popescu, K. Badizadegan, R. R. Dasari, and M. S. Feld, "Fresnel particle tracing in three dimensions using diffraction phase microscopy," Opt. Lett. **32**(7), 811–813 (2007).
23. B. Xiao, J. F. Ma, and X. Wang, "Image analysis by Bessel-Fourier moments," Pattern Recognit. **43**(8), 2620–2629 (2010).
24. I.-K. Lee, "Curve reconstruction from unorganized points," Comput. Aided Geom. Des. **17**(2), 161–177 (2000).
25. M. Speidel, A. Jonás, and E. L. Florin, "Three-dimensional tracking of fluorescent nanoparticles with subnanometer precision by use of off-focus imaging," Opt. Lett. **28**(2), 69–71 (2003).
26. M. Kvarnström and C. A. Glasbey, "Estimation of centres and radial intensity profiles of spherical nanoparticles in digital microscopy," Biometrical J. **49**(2), 300–311 (2007).
27. F. C. Cheong, K. Xiao, D. J. Pine, and D. G. Grier, "Holographic characterization of individual colloidal spheres' porosities," Soft Matter **7**(15), 6816–6819 (2011).
28. U. Piran and W. J. Riordan, "Dissociation rate constant of the biotin-streptavidin complex," J. Immunol. Methods **133**(1), 141–143 (1990).
29. S. G. Sun, X. Huang, M. H. Ma, N. Qiu, Z. X. Cai, Z. Luo, and N. P. Alies, "Systematic evaluation of avidin-biotin interaction by fluorescence spectrophotometry," Spectrochim. Acta A Mol. Biomol. Spectrosc. **89**, 99–104 (2012).
30. X. Fan, I. M. White, S. I. Shopova, H. Y. Zhu, J. D. Suter, and Y. Z. Sun, "Sensitive optical biosensors for unlabeled targets: A review," Anal. Chim. Acta **620**(1–2), 8–26 (2008).
31. S. Przibilla, S. Dartmann, A. Vollmer, S. Ketelhut, B. Greve, G. von Bally, and B. Kemper, "Sensing dynamic cytoplasm refractive index changes of adherent cells with quantitative phase microscopy using incorporated microspheres as optical probes," J. Biomed. Opt. **17**(9), 0970011 (2012).
32. Á. Barroso, M. Woerdemann, A. Vollmer, G. von Bally, B. Kemper, and C. Denz, "Three-dimensional exploration and mechano-biophysical analysis of the inner structure of living cells," Small **9**(6), 885–893 (2013).
33. F. Strubbe, F. Beunis, T. Brans, M. Karvar, W. Woestenborghs, and K. Neyts, "Electrophoretic retardation of colloidal particles in nonpolar liquids," Phys. Rev. X **3**(2), 021001 (2013).
34. F. Beunis, F. Strubbe, K. Neyts, and D. Petrov, "Beyond Millikan: the dynamics of charging events on individual colloidal particles," Phys. Rev. Lett. **108**(1), 016101 (2012).
35. J. A. van Heiningen and R. J. Hill, "Polymer adsorption onto a micro-sphere from optical tweezers electrophoresis," Lab Chip **11**(1), 152–162 (2011).
36. G. S. Roberts, R. Sanchez, R. Kemp, T. Wood, and P. Bartlett, "Electrostatic charging of nonpolar colloids by reverse micelles," Langmuir **24**(13), 6530–6541 (2008).
37. G. N. Smith and J. Eastoe, "Controlling colloid charge in nonpolar liquids with surfactants," Phys. Chem. Chem. Phys. **15**(2), 424–439 (2013).
38. M. F. Hsu, E. R. Dufresne, and D. A. Weitz, "Charge stabilization in nonpolar solvents," Langmuir **21**(11), 4881–4887 (2005).
39. S. K. Sainis, J. W. Merrill, and E. R. Dufresne, "Electrostatic interactions of colloidal particles at vanishing ionic strength," Langmuir **24**(23), 13334–13337 (2008).
40. A. E. Cohen, "Control of nanoparticles with arbitrary two-dimensional force fields," Phys. Rev. Lett. **94**(11), 118102 (2005).

1. Introduction

Colloidal particles are widely used in pharmaceutics [1,2], flow cytometric assays [3], biophysics [4–6], liquid toners and electronic inks [7,8], photonics [9,10] and soft condensed matter [11]. In many of these applications it is desired to know accurate particle properties such as size, refractive index, shape and electrical charge, properties of coatings on these particles or statistical properties of many particles. Commonly used methods to characterize particles like dynamic light scattering, disc centrifugation or Doppler velocimetry [12], and single-particle based methods such as electron microscopy, particle tracking [13,14], laser backscattering [15], holographic microscopy [16,17] have their differences in resolution,

#220421 - $15.00 USD Received 5 Aug 2014; revised 17 Sep 2014; accepted 21 Sep 2014; published 1 Oct 2014

number of parameters that can be measured, ability to measure polydisperse particle samples, measurement speed and cost.

In this paper we demonstrate the Fourier-Bessel Image Decomposition method (FBID) based on Fourier-Bessel (FB) image moments which combines the benefits of an ordinary microscopy setup and accurate particle-based measurements of size, refractive index (RI) and 3-dimensional position. The FBID method can be situated between methods that extract just the intensity centroid or a few higher order intensity moments [18–21] and methods that completely fit the image data to simulations of the Mie theory [16,17]. In the FBID method, particle images obtained by classical white light, fluorescence, confocal microscopy or any other imaging technique are decomposed into a set of 2-dimensional orthogonal FB functions with their weights, the FB-coefficients. Since each image can then be represented by a point in the multidimensional space of FB-coefficients the mathematical processing becomes much easier compared to analyzing the original images. Many images of a particle at different z-positions with respect to the plane of focus result in a point cloud, an 'optical fingerprint', that accurately reflects is size and refractive index. The limits of the resolution are explored by measuring monodisperse particles with known size and refractive index, as well as by investigating the binding of avidin to biotinylated particles [21]. The disadvantage of the FBID method is that calibration with particles of known properties is required to achieve quantitative results on size and refractive index. Therefore the accuracy of the results is limited by the calibration particles. For spherical particles the optical fingerprint of the FB coefficients forms a curved line and the distance along this line is a monotonous function of the particle z-position. Therefore the FBID method is convenient for 3-dimensional out-of-focus tracking of all kinds of particles such as fluorescent nanoparticles [22]. For absolute measurements of the z-position a theory is developed to calibrate the monotonous function of the z-position from the statistics of the particle's Brownian motion.

2. Materials

In our setup images of colloidal particles are acquired with a Nikon Eclipse Ti microscope at 100 × objective magnification (NA 1.3) and an Andor iXon$^+$ EM-CCD camera at 25 Hz. A 12V/100W halogen lamp and a CLWD condenser with NA 0.72 are used for Köhler illumination. The focal plane is set in the channel of a microfluidic device (1 μ-Slide VI 0.4 uncoated from IBIDI) at 60 micrometer above the bottom interface. The microfluidic channel is filled with monodisperse dispersions of polystyrene (PS) and poly(methyl methacrylate) (PMMA) particles in the size range between 500 nm and 1300 nm (see Table 1). All particles except the biotinylated PS are dispersed in de-ionized water at volume fractions around 0.001. The nominal diameter d is the mean diameter obtained by the manufacturer using disc centrifuging. The PS particles with d = 899 nm and 990 nm are from Polysciences, the other PS and PMMA particles are from Microparticles GmbH. The biotinylated PS microparticles of nominal diameter d = 1031 ± 25 nm (Life Technologies) are received as 1% solids dispersion in a 0.4 mL aqueous dispersion with 50mM sodiumphosphate, 50 mM NaCl, 0.02% Tween 20 and 5 mM sodium azide. Avidin (Novex) is received from Life Technologies as 10 mg powder. Two 2 ml dispersions are made in Dulbecco's phosphate buffered saline (DPBS) buffer: one with and one without avidin. Both dispersions contain 0.018 mg biotinylated PS particles (volume fraction $\phi = 10^{-5}$) and 0.1% Tween 20. One dispersion contains no avidin while the other contains 0.147 mg avidin. According to the specifications provided by Life Technologies the avidin-binding capacity of the biotinylated PS particles is 13.3 nmoles avidin per mg particles, corresponding to 0.88 mg avidin per mg particles. Therefore, our sample with 0.018mg particles and 0.147mg avidin contains sufficient avidin to fully saturate all biotinylated PS particles.

#220421 - $15.00 USD Received 5 Aug 2014; revised 17 Sep 2014; accepted 21 Sep 2014; published 1 Oct 2014

Table 1. Particle Sizes of Monodisperse PS and PMMA Particles Provided by the Manufacturer

material	Mean diameter *d* (nm)	Standard deviation (nm)
PS	522	12
PS	721	20
PS	899 ± 11	31
PS	940 ± 15	17
PS	990 ± 10	30
PS	1046 ± 16	35
PS	1270	30
PMMA	601	14
PMMA	807	19
PMMA	1020	40
PMMA	1230	40
biotinylated PS	1031	25

3. Fourier-Bessel image decomposition method

N images (typically 1000) are acquired for each measured particle, while it is performing free Brownian motion. Only images are used in which the particle image is not influenced by neighbouring particles. In each image, after background subtraction, the sub-pixel intensity weighed centroid is calculated [18]. Then, a FB series expansion [23] of each image is calculated using the following set of 2-dimensional polar FB functions $\Psi_{m,n}(r,\varphi)$ in the polar coordinates r and φ:

$$\Psi_{n,m}(r,\varphi) = \frac{1}{\sqrt{2\pi N_n^{(m)}}} J_m\left(x_{mn} r/a\right) e^{im\varphi} \tag{1}$$

The FB functions form an orthonormal set in the *r*-interval $[0,a]$. They are set equal to zero outside of the interval $[0,a]$ and with zero-boundary condition at $r = a$. J_m is the *m*-th order Bessel function of the first kind with positive zeros x_{mn}, and with $N_n^{(m)} = a^2 J_{m+1}^2\left(x_{mn}\right)/2$. In our experiments a = 20 pixels is the chosen cut-off radius, where 1 pixel corresponds to 80 nm in the plane of focus. The FB coefficients $B_{m,n}$ are obtained by convolution of the image with the FB functions:

$$B_{m,n} = \sum_{i,j} I\left(i,j\right) \Psi^*_{m,n}\left(i,j\right). \tag{2}$$

Here, $I(i,j)$ are the normalized and background-corrected image pixels. $\Psi^*_{m,n}(i,j)$ are the discretized values of the Fourier-Bessel functions $\Psi_{m,n}(r,\varphi)$ of order (*m*,*n*) centered at the sub-pixel centroid location. In the next only the coefficients $B_{0,n}$ for which $m = 0$ are used since for spherical particles the coefficients with $m \neq 0$ are small and contain no useful information. For the study of non-spherical particles however these coefficients with $m \neq 0$ are important to obtain the particle shape and orientation.

As a result, each particle image $I(i,j)$ is transformed into a $(m \times n)$-dimensional point. For spherical particles a sequence of *N* images acquired at different *z*-positions forms a point-cloud scattered along a multidimensional curve. With a point linking algorithm [24] a piecewise linear curve *S* is fitted to the scattered data. By projecting data points on the curve *S*, the distance *s* along the curve is obtained which is a monotonous function of the *z*-position, as well as the distance ε between the data point and *S* which is related to the measurement error.

#220421 - $15.00 USD Received 5 Aug 2014; revised 17 Sep 2014; accepted 21 Sep 2014; published 1 Oct 2014

4. Results

Figure 1 shows 10 FB coefficients $B_{0,n}$ for $n = 1,\ldots,10$ and $m = 0$ of a single particle (899 nm, PS) as a function of s. The value $s = 0$ corresponds to the highest and $s \cong 24$ to the lowest measured z-position of the particle. The piecewise linear curve S is shown as a black line as well. Three particle images (with enhanced contrast for clarity) are shown with their corresponding s-positions. The scattering error is due to background noise, errors in the intensity centroid and errors related to discretization of the FB functions. The standard deviation of the scattered experimental data around the curve S decreases for the different modes $n = 1,2,\ldots,10$: 0.092, 0.038, 0.042, 0.038, 0.038, 0.023, 0.015, 0.013, 0.012, 0.011 together with the average amplitude of the coefficients (except for $n = 1$): 1.3779, 1.7127, 1.4513, 0.8576, 0.3869, 0.2323, 0.1603, 0.1192, 0.1037, 0.0888. The best signal-to-noise ratio is observed for modes $n = 2$, 3 and 4, which means that selecting modes can increase the accuracy of any further analysis. The average value for ε (the multidimensional distance between data points and the piecewise linear curve S) for $n = 1{:}10$ and over all s-positions is 0.11.

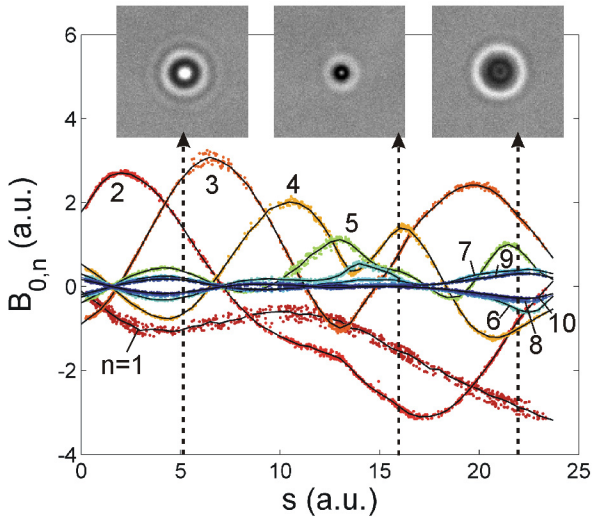

Fig. 1. The optical fingerprint of a 899 nm PS particle consisting of 10 FB-coefficients $B_{0,n}$ with $n = 1,\ldots,10$ as a function of the position s along the fitted piecewise linear curve S. Original particle images (with enhanced contrast) are shown at three s-positions.

The transformation of images to the multidimensional space of FB-coefficients offers the advantage that a monotonous function of the z-position is readily obtained, making it convenient for out-of-focus particle tracking over a large range of z-positions and for calibrating the absolute z-position prior to further measurements (for example of the electrophoretic mobility). It offers a more general approach to 3D-tracking than linking a particular feature like for example the distance from the center to the outermost ring of the image of a fluorescent nanoparticle to its z-position [25]. The FBID method can be used with different types of illumination and imaging such as fluorescence, confocal or holographic microscopy. With the Köhler illumination used in our experiments the maximal distance from the plane of focus that a 1 µm particle can be tracked is about 10 µm. The range of the out-of-focus tracking and the lateral resolution of the particle tracking can be further increased by using other types of imaging such as holographic imaging. Figure 2 shows the value of s as a function of time for the particle measured in Fig. 1. For a spherical particle performing Brownian motion and knowing that $z(s)$ is a monotonous function of s that has to satisfy Brownian statistics it is possible to reconstruct the z-position quite accurately. From the 2-

#220421 - $15.00 USD Received 5 Aug 2014; revised 17 Sep 2014; accepted 21 Sep 2014; published 1 Oct 2014

dimensional Brownian motion parallel to the plane of focus [13] or from the size calculation described below the diffusion constant D is calculated. The motion in the z-direction should therefore satisfy the statistic $\left\langle (\Delta z)^2 \right\rangle = 2D\Delta t$ at every position z, where Δz is a displacement in the z-direction in the time Δt. The transformation from s to z is given by: $z(s) = \int \sqrt{2D\Delta t} \Big/ \sqrt{\left\langle \Delta s^2 \right\rangle (s)} ds$ where $\left\langle \Delta s^2 \right\rangle (s)$ is the s-dependent mean squared displacement of s in the time-interval Δt. In practice the average value of Δs^2 is calculated in discrete intervals and $z(s)$ is calculated by numerical integration of these averages. The reconstructed z-position and the transformation formula $z(s)$ (inset) are shown in Fig. 2. The relative error on $\left\langle \Delta s^2 \right\rangle (s)$ scales with $\sqrt{2/M}$ where M is the number of measurements of Δs^2 in the interval around s. Therefore the error on the reconstructed z-position relative to a known reference position z_0 is $\sigma_{\Delta z} = \Delta z \sqrt{2/N_1}$, where $\Delta z = z - z_0$ and N_1 is the number of data points obtained in the interval between z_0 and z assuming that they are evenly distributed over these intervals. This means that small, local particle movements Δz are accurately reproduced, while particle motion over a larger distance becomes less accurate. For a typical experiment this gives an absolute accuracy of 5 nm over 100 nm displacements and an accuracy of 50 nm over 1-micrometer displacements in the z-direction. Complementary ways to obtain $z(s)$ with a z-scan method by moving the microscope stage [18,26] can result in better accuracies in the z-position.

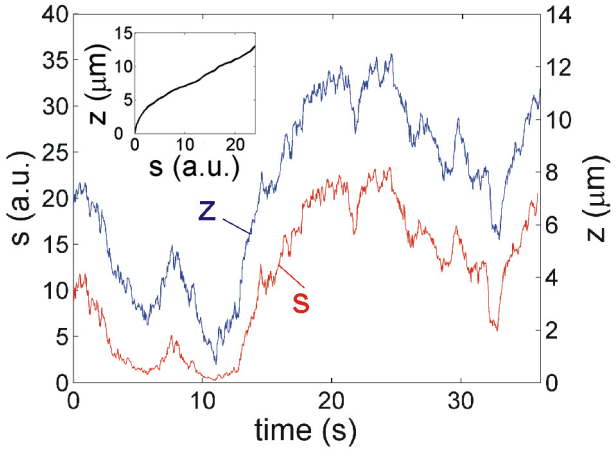

Fig. 2. Using the same particle as shown in Fig. 1 performing Brownian motion. The distance s of the projection of the coefficients $B_{0,n}$ onto the piecewise linear curve S is shown as a function of time. Using Brownian statistics the monotonous function z(s) is calculated to convert the s–position into the relative z-position of the particle.

Now the particle size is investigated. In single particle tracking experiments the particle radius R_D is often calculated from Brownian motion using Stokes law for a sphere: $R_D = kT/6\pi\eta D$, with k the Boltzmann constant, T the temperature, η the viscosity. Due to the inherent stochastic nature of Brownian motion the relative accuracy on the measured value D is $1/\sqrt{N}$ with N the number of particle positions. Therefore in our experiments with N = 1000 the accuracy on R_D is 3% which corresponds to an error of ± 16 nm on a particle with radius R = 500 nm. Using the FB-coefficients, the size can be determined with high precision

#220421 - $15.00 USD Received 5 Aug 2014; revised 17 Sep 2014; accepted 21 Sep 2014; published 1 Oct 2014

not limited by Brownian stochastics but limited only by the image quality (which determines resolving power) and the calibration procedure (which determines the absolute accuracy). Let us first investigate the resolving power of the particle size. Particles with a different size have *S*-curves that are shifted with respect to each other. For example the *S*-curve at the point s = 10 of the data in Fig. 1 for a particle of d = 899 nm shifts with about 1 unit per 55 nm change in particle radius (data similar to shown in Fig. 3(a)). Therefore the error ε = 0.11 on a single data point corresponds to an accuracy (standard deviation) on the radius of 0.11 × 55 nm = 6 nm, which gives a relative size error of 1.3%. And by selecting only modes with high signal-to-noise ratio (e.g. $B_{0,2}$, $B_{0,3}$ and $B_{0,4}$) the resolution drops just below 1%. Therefore here the resolution or discriminating power between different particle sizes is more accurate than can be achieved by analyzing 1000 images of Brownian motion. The size-resolution depends on the position along the *S*-curve, and is lower than 1% for particles further away from the plane of focus. It is important to stress that the single-particle accuracy reflects resolving power (the minimal difference in radius that can be resolved), and not the absolute accuracy in size which is limited by the accuracy of the size-calibration.

Since there is no theoretical formula for the radial intensity profile of a particle under Köhler illumination and since we want to avoid simulations, we resort to empirical methods to calibrate the size. The size-calibration can be achieved either by measuring monodisperse particles of known average size (from DLS, disc centrifugation or other techniques), or by measuring the Brownian motion of particles to calculate their average size with Stokes law. Both techniques are limited in accuracy (a batch of 'monodisperse' particles typically has a 10% standard deviation in the size) and are sensitive to errors (the accuracy of Browian motion analysis depends on the number of images), which limits the accuracy of the overall size-calibration. The size-calibration of individual particles is illustrated in Fig. 3(a), showing *S*-curves of particles from the PS particle dispersions with nominal diameter d = 899, 940, 990 and 1046 nm. Only two components ($B_{0,2}$ and $B_{0,3}$) are shown for clarity, but the calculations are done with all 10 FB coefficients. The vector T was created roughly perpendicular to the *S*-curves and pointing in the direction of increasing particle size in a chosen region with high size resolution. The original data-points belonging to the different particles within a cylinder of radius 0.3 are projected onto T resulting in a position t. The average distances t = 0, 0.60, 1.07, 1.70 corresponding to the particle sizes d = 899, 940, 990 and 1046 nm are used for the size-calibration.

For determining the size of a particle, the projected value t of a data point can be transformed into a size by linear interpolation of the calibrated values. Figure 3(b) shows the average diameter and standard deviation for each particle used for the calibration. Per particle typically 10 data points are used. The standard deviation on the particle diameter is around 4 nm corresponding to a relative error of 0.4%. The overall size histogram in Fig. 3(c) shows that the 4 particle sizes are resolved well. The accuracy of the method is sufficient to reliably represent the particle size polydispersity. For comparison, the size-data obtained from Brownian motion analysis has an 8 times higher standard deviation on the size, such that the 4 particle diameters d = 899, 940, 990 and 1046 nm are not resolved. DLS experiments typically need a factor two difference in size in order to resolve particle sizes. With DLS, for example the sample with d = 899 nm particles showed a 100 nm wide peak (corresponding to a resolution of 6%) and a mixture of 4 particle sizes d = 899, 940, 990 and 1046 nm was not resolved.

#220421 - $15.00 USD Received 5 Aug 2014; revised 17 Sep 2014; accepted 21 Sep 2014; published 1 Oct 2014

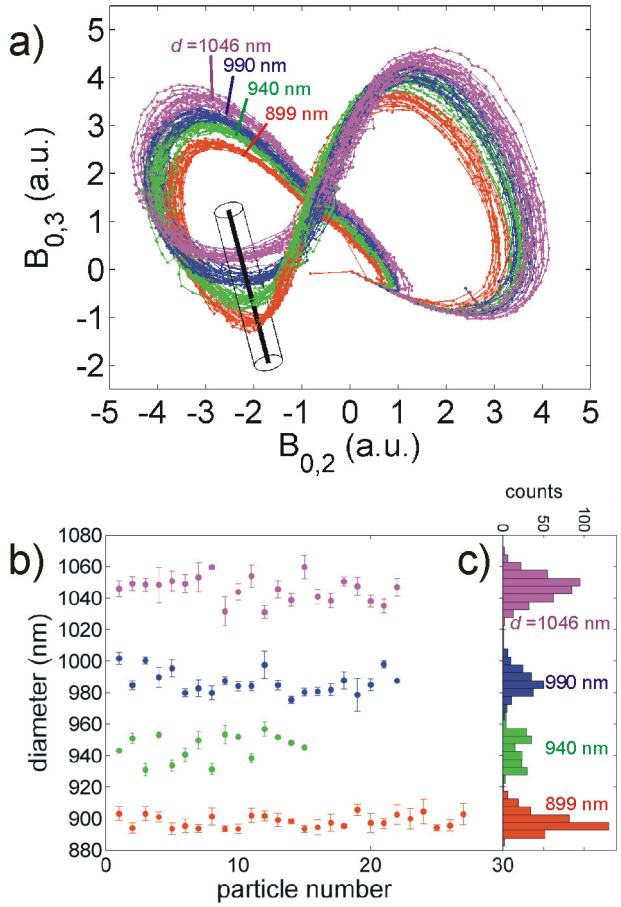

Fig. 3. (a) *S*-curves of PS particles (here only 2 components $B_{0,2}$ and $B_{0,3}$ are shown) show a clear shift with increasing diameter d = 899, 940, 990 and 1046 nm. Projection of original FB-coefficients in the cylinder onto the line T is used for calibration. In (b) the interpolated sizes for different particles are shown. The typical single-particle radius accuracy is around 5 nm (~ = 1%). In (c) the overall size histogram shows that the 4 particle sizes are resolved well.

Similar to the size also the refractive index of particles is calculated based on interpolation with calibration data. Figure 4 shows the projection of 3 Fourier-Bessel coefficients ($B_{0,2}$, $B_{0,3}$ and $B_{0,4}$) from various particles on a plane U with orthogonal basis u and v. The plane U is chosen roughly orthogonal to the *S*-curves and at a position along the *S*-curves with maximal resolution in the size and refractive index. The PS (n_p = 1.59) particles with d = 522, 721, 899, 940, 990, 1046 and 1270 nm form a line that is shifted with respect to the line from PMMA particles (n_p = 1.49) with d = 601, 807, 1020 and 1230 nm. Under the assumption that there is no refractive index polydispersity the RI resolution is estimated for the PS particles of d = 990 nm by projecting the corresponding data points in the (u,v)-plane on a line between the average values of the PS particles of 990 nm and the PMMA particles of 1020 nm, which results in distances along that line. The standard deviation of these distances is compared to the distance between the average values of PS and PMMA particles which corresponds to a RI difference of 0.1. For the PS particle around d = 1000 nm the RI resolution is about 0.0025. Interestingly, a detailed study of the refractive index of similar PS particles shows a RI polydispersity of roughly 0.002 [27], indicating that the intrinsic RI

#220421 - $15.00 USD Received 5 Aug 2014; revised 17 Sep 2014; accepted 21 Sep 2014; published 1 Oct 2014

resolution from our measurements could be below 0.0025 RIUs. It can be observed that the RI resolution decreases for smaller particles.

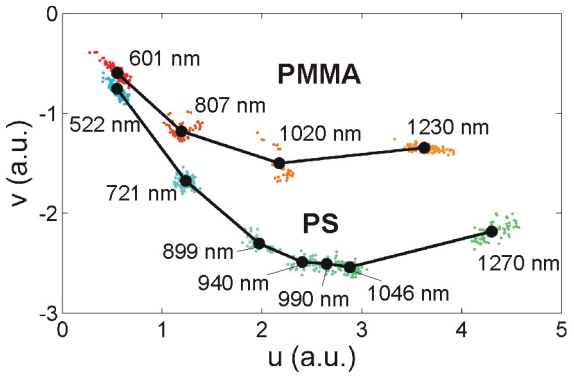

Fig. 4. The projection is shown of three FB-coefficients ($B_{0,2}$, $B_{0,3}$ and $B_{0,4}$) with distance from the plane U closer than 0.2 onto that plane with orthonormal axes u and v. The groups of points from PS (n_p = 1.59) and PMMA (n_p = 1.49) particles show two distinct lines for increasing particle sizes. The RI resolution for particles of d = 1000 nm is around 0.0025.

Finally, the binding of avidin molecules to biotinylated PS particles is investigated using the FBID method. For this experiment two particle samples with biotinylated PS particles were prepared in DPBS buffer: one without and one with avidin (see Materials). The nominal particle diameter is d = 1.031 ± 0.025μm. The affinity between avidin and biotin is very strong [28,29]. The avidin concentration is 8 times larger than the maximum binding capacity of the biotinylated PS particles specified by Life Technologies, such that all biotin molecules are expected to be saturated with avidin. If the avidin was distributed homogeneously in the liquid the concentration would be too low to have any influence on the refractive index of the liquid medium. However, a biotinylated PS particle fully covered with avidin contains roughly 5×10^6 avidin molecules on its surface. As a result the particle size increases roughly by two nanometers and the effective refractive index of the particle is expected to change by about 2×10^{-3} RIU's, which is just detectable with the FBID method. Figure 5(a) shows the FB-coefficients $B_{0,2}$ and $B_{0,3}$ for 3 representative particles without avidin (green) out of a total of 41 particles and 3 representative particles with avidin (red) out of a total of 49 particles. Per particle 1000 images are obtained and analyzed. A small but significant shift can be observed in the optical fingerprints for particles with and without avidin. However, due to size polydispersity and other errors, there is quite some scattering on the data. Therefore a statistical analysis of the complete data restricted to parameters $B_{0,2}$, $B_{0,3}$ and $B_{0,4}$ is carried out, focusing on those regions with the most significant shift in the optical fingerprints (the two regions indicated between arrows in Fig. 5(a). First, the average fingerprints of all particles without avidin S_0 and for all particles with avidin S_1 are obtained (full and dotted lines in Fig. 5(a). Next, a set of vectors T perpendicular to S_0 is constructed with origin at different positions s along curve S_0 and with endpoint on S_1. For each vector T, the coordinate t is the distance along each vector, with t = 0 on curve S_0 and t = 1 on curve S_1. Now, when a data point is projected onto the closest vector T a value of t is obtained. For each particle the normalized separation t is then calculated as the average of all values t for all of its data points. Figure 5(b) shows the normalized separation t which has an average value zero with standard deviation 0.34 for the particles without avidin, and an average value of 1 with standard deviation 0.46 for the particles with avidin. A T-test with these values confirms that there is a significant shift in the data from particles with and without avidin bound to the biotinylated surface. The standard deviation on t for each individual particle is limited by image noise and is 0.16 for data without avidin and 0.24 for data with avidin.

#220421 - $15.00 USD Received 5 Aug 2014; revised 17 Sep 2014; accepted 21 Sep 2014; published 1 Oct 2014

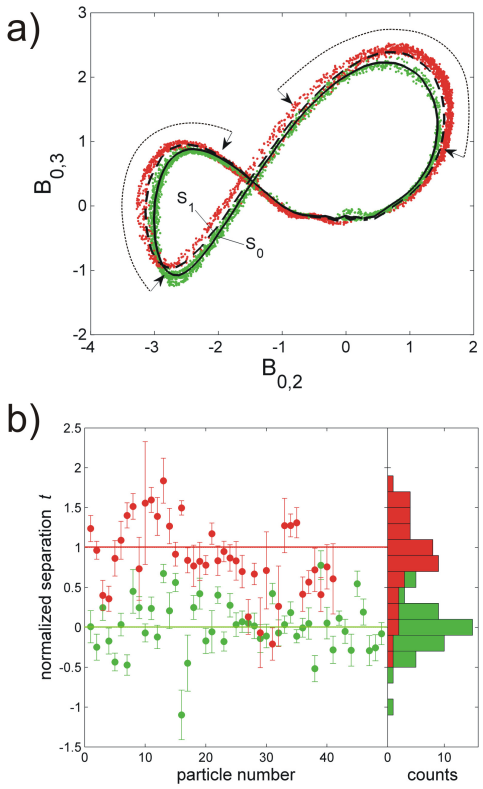

Fig. 5. (a) The FB-coefficients $B_{0,2}$ and $B_{0,3}$ are shown for 3 biotinylated particles without avidin (green) and with avidin (red). The average of all 41 particles without avidin S_0 (black line) and of all 49 particles with avidin S_1 (dotted line) are shown. (b) The normalized separation t for each particle is calculated based on coefficients $B_{0,2}$, $B_{0,3}$ and $B_{0,4}$, where t = 0 corresponds to S_0 and t = 1 corresponds to S_1.

5. Discussion

The FBID method provides a framework for analyzing all kinds of colloidal particles under various illumination and imaging conditions such as in fluorescence, confocal or holographic microscopy. Besides spherical micrometer-sized particles as studied here also fluorescent, nanometer-sized, core-shell, absorbing or non-spherical particles can be analyzed. Axisymmetrical particles and arbitrarily shaped particles can be analyzed to obtain size-, shape- and orientational information by including azimuthal FB-functions. However, the characterization of the size and refractive index of particles with the FBID method is limited to particles larger than a few hundred nm, since the accuracy drops rapidly for particle diameters below 300 nm. Quantitative results on the size and refractive index are also limited by the quality of the particles used for calibration. The demonstrated out-of-focus tracking algorithm can be used even for particles smaller than 300 nm and provides a more general framework compared to existing z-position algorithms for nanoparticles [25].

The FB decomposition of particle images is fast enough for real-time processing at 100 Hz. In the analysis of the size and refractive index the calibration procedure is the most time consuming step. In our experiments the calibration data is obtained from particles performing Brownian motion. Then, it takes a few tens of minutes to acquire sufficient calibration data, since several particles dispersions have to be loaded and for each dispersion many particles are filmed for a few seconds. This collection of calibration data can be sped up using directed

#220421 - $15.00 USD Received 5 Aug 2014; revised 17 Sep 2014; accepted 21 Sep 2014; published 1 Oct 2014

liquid flow to scan the particle *S*-curves faster. The averaging of the calibration data and the interpolation to obtain particle properties can be achieved in a few minutes.

For determining particle properties such as the size and refractive index, the FBID method requires a one-time calibration with a few well-known particles. As shown in the examples, a few tens of particles and roughly 1000 images per particle are required for the calibration. Such a calibration procedure would not be necessary when the method could rely on detailed Mie-scattering simulations [16,17] that take into account the optical properties of the illumination and detection systems and the shape and optical properties of the particles. In this case the FBID method would be able to analyze single images and might be suitable for quantitative measurement and comparison of colloidal particles. The parameter fitting could then be based on the multidimensional point in the FB coefficient space. However, such Mie-scattering simulations including for example Köhler illumination and non-spherical, core-shell, fluorescent or absorbing particles are difficult and time-consuming, which is avoided when using the FBID method.

The demonstrated resolution of about 10^{-3} RIU is nowhere near the 10^{-7} to 10^{-8} RIU resolution of current biosensors based on surface plasmon resonance, ring resonators and microsphere resonators [30]. Still, the observation of a significant shift in the optical fingerprints between biotinylated PS particles with and without avidin shows that the FBID method can be useful for investigating antibody-antigen interactions at the surface of single microparticles, the growth of coatings on particles and the dissolving process of particles [21]. To eliminate errors related to polydispersity it makes sense to investigate the dynamics of the avidin-biotin binding process on a single probe particle.

In applications of the FBID method the particles can be the objects of interest. Then, their size, refractive index, shape and orientation, coatings and other properties can be investigated [1,2]. In other applications they are used as probe particles to monitor the local refractive index of liquids [5], as intracellular probes inside cells for biomedical applications [31,32], for fundamental electrokinetics [33], for studying the elementary chemical reactions and molecule adsorption at the particle-liquid interface [34,35], charging behavior of colloids [36,37], inter-particle interactions [38,39] and for electrical trapping [40].

6. Conclusions

We demonstrated that the FBID method can be used to determine the 3-dimensional position, size and refractive index of single colloidal spheres using appropriate calibration. The *s*-position, a monotonous function of the *z*-position easily obtained without any calibration, is used for out-of-focus particle tracking. For particles performing Brownian motion the Brownian statistics can be used to obtain the absolute *z*-position with nanometer precision on short displacements. The method allows measuring the particle size with resolution 1% and the refractive index with resolution of 0.4%. This is particularly useful for characterizing polydisperse micrometer-sized colloids and for characterizing colloidal probes in various experiments. The limitations in the resolution of the FBID method are explored by measuring the binding of avidin molecules to biotinylated particles.

Acknowledgments

This research was supported by the Research Foundation – Flanders (FWO Vlaanderen), IWT-Vlaanderen, the IAP project photon@be funded by the Belgian Science Policy program and the Hercules Foundation.

#220421 - $15.00 USD Received 5 Aug 2014; revised 17 Sep 2014; accepted 21 Sep 2014; published 1 Oct 2014